SSRG International Journal of Geo-informatics and Geological Science
ISSN: 2393–9206 / https://doi.org/10.14445/23939206/IJGGS-V13I2P101

Volume 13 Issue 2, 1-12, May-Aug 2026

Original Article

ASTER-PCA for Lithological Discrimination in Holenarsipura Schist Belt (HSB), Dharwar Craton, Karnataka, India

Shubhachintani Bhukta[1], Basavarajappa H. T[1], Manjunatha M. C[2], Sadiq Ali Nawabi[3]

[1,3]*Department of Studies in Earth Science, CAS in Precambrian Geology, University of Mysore, Mysuru, India.*
[2]*DBT-Builder, Department of Community Medicine, JSS Medical College, JSS AHER, Mysuru, India.*

[1]*Corresponding Author : shubhachintanibhukta@gmail.com*

Received: 07 May 2026 Revised: 09 June 2026 Accepted: 26 June 2026 Published: 08 July 2026

Abstract *- Lithological discrimination in complex Precambrian terrains is important for understanding geological evolution and assessing mineral resource potential. This study evaluates the effectiveness of Principal Component Analysis (PCA) applied to multispectral ASTER data for lithological mapping in Holenarasipur Schist Belt of Western Dharwar Craton. Although ASTER- and PCA-based lithological studies have been carried out in different parts of the Dharwar Craton and Karnataka, their application to the Holenarasipur Schist Belt remains limited. ASTER Level-1T VNIR and SWIR datasets were processed using PCA to reduce spectral redundancy and enhance lithological contrasts. The derived principal components were examined to identify the spectral behavior of major lithological units, and selected RGB composites were generated for geological interpretation. Field validation was carried out using representative rock samples collected along the NE–SW-trending schist belt. Among the derived components, PC-2, PC-3, and PC-4 were the most useful for lithological discrimination. PC-2 highlighted iron-bearing formations such as banded magnetite quartzite, whereas PC-3 enhanced silica-rich lithologies, including gneisses and granitoids. PC-4 emphasized hydroxyl- and magnesium-bearing units such as ultramafic rocks and talc schists. The RGB composite generated from these components clearly differentiated the main lithological units, and field observations showed good agreement with the satellite-based interpretation. The results indicate that PCA of ASTER multispectral data provides a practical, efficient, and cost-effective approach for lithological mapping and mineral exploration in complex Precambrian terrains.*

Keywords *- ASTER Image Interpretation, PCA, Precambrian Terrain, Spectral Enhancement Technique, VNIR--SWIR Bands.*

1. Introduction

Lithological maps form the base for most geological interpretations. They help in recognising the distribution of rock units, tracing structural trends, and assessing areas of mineral potential [37][16]. In practice, such maps are best prepared through field observations, but field mapping alone is not always adequate in Precambrian terrains. The rock exposures in such terrain are often discontinuous, strongly weathered, locally masked by soil or vegetation, and modified by multiple phases of deformation and metamorphism. As a result, mapping large or difficult areas only by ground survey can be slow, costly, and spatially incomplete [11]. Satellite remote sensing is useful in this situation because it gives a synoptic view of the terrain and allows regional lithological patterns to be examined before and during field verification [23].

Among the available multispectral sensors, the Advanced Spaceborne Thermal Emission and Reflection Radiometer (ASTER) has been widely used in geological studies. Its Visible and Near-Infrared (VNIR), Shortwave Infrared (SWIR), and Thermal Infrared (TIR) bands record spectral responses that are closely related to mineral composition [42][1]. Minerals containing iron, hydroxyl groups, carbonate, silicate, and quartz commonly show diagnostic behaviour within these wavelength regions [9]. This makes ASTER suitable for distinguishing lithological units and alteration zones, especially where the surface exposure is sufficient. Earlier work has shown that ASTER data can help separate carbonate, silicate, quartz-rich, mafic, ultramafic, and granitoid rocks, and in some cases can provide clearer geological information than older multispectral datasets such as Landsat TM [29].

The usefulness of ASTER data, however, depends strongly on how the spectral information is processed. In structurally complex and weathered terrains, the original bands may not show clear differences between rock types. A

single lithology may display variable reflectance because of slope, weathering, soil cover, or vegetation, while different lithologies may appear spectrally similar. Therefore, enhancement methods are required to emphasise subtle spectral contrasts. Principal Component Analysis (PCA) is one such commonly used spectral enhancement technique. It transforms correlated multispectral bands into uncorrelated components, allowing the main spectral variations to be separated into fewer images [10][36]. For geological mapping, this is useful because selected principal components may enhance weak lithological signals, reduce repeated band information, and help interpret contacts, faults, alteration zones, and rock-unit boundaries. Although band-ratio images and Decorrelation Stretch can improve spectral contrast, PCA is especially useful for separating subtle lithological variations that are not clearly expressed in traditional colour composites [8].

Several studies have used ASTER-PCA approaches for geological mapping in different terrains. In the western United States and Iran, ASTER-based processing has helped discriminate mafic--ultramafic rocks, granitoids, sedimentary units, and mineralised zones [43][31]. Similar work from Egypt has shown the value of ASTER methods for mapping ophiolitic assemblages, hydrothermal alteration zones, and related lithological units [3]. These examples show that the method is particularly useful where bedrock is exposed, and lithological units have measurable VNIR--SWIR spectral differences. Recent studies also show that PCA and related ASTER-based enhancement methods remain useful for delineating geological units in complex areas [5][12]. Other recent work has also reported improved mineralogical or lithological discrimination using comparable enhancement approaches [30]. These applications indicate that PCA can preserve meaningful spectral variation while reducing redundant information and noise [15]. Although machine-learning methods are increasingly used for automated lithological classification, they often require large, well-distributed training datasets [26][38]. PCA, therefore, remains important as a transparent and practical method, particularly in areas where field control is limited and the first task is to identify which spectral components best express lithological variation.

In India, remote sensing has been applied to many geological provinces, including the Aravalli--Delhi orogenic belt, the Deccan volcanic province, and the Dharwar Craton [16]. ASTER SWIR-based studies from areas such as Udaipur, Rajasthan, have shown that PCA, Minimum Noise Fraction (MNF), and Independent Component Analysis (ICA) can assist in separating lithological units and mineral deposits [34]. In southern India, remote sensing data have been used to map schist belts, granitoids, and alteration zones in Precambrian terranes [22][35]. Work from Karnataka has also shown the value of spectral data for recognising major litho-units in schist-belt settings [25]. Even with these contributions, many studies have concentrated on regional mapping or mineral-alteration targets. ASTER- and PCA-based work has been carried out in different parts of the Dharwar Craton, and Karnataka [6] [25], but a detailed evaluation of PCA-derived ASTER components for lithological discrimination in the Holenarasipur Schist Belt is still limited.

The Holenarasipur Schist Belt represents one such challenging terrain. It is part of the Dharwar Craton and includes greenstone, ultramafic, mafic, granitoid, and gneissic units [27][33]. The belt is geologically important, but its lithological units are not always easy to separate on satellite imagery. Many exposures are narrow or discontinuous, and the spectral signatures of different rocks may overlap because of metamorphism, deformation, weathering, vegetation, and surface cover. These conditions make the area a suitable case for testing whether PCA can improve the visibility of lithological differences in ASTER data.

The present study addresses this gap by evaluating ASTER-based PCA for lithological discrimination in the Holenarasipur Schist Belt. While ASTER and PCA have been tested in several parts of Karnataka, the Dharwar Craton, and other geological settings, their usefulness for this particular schist belt terrain has not been clearly demonstrated. The main contribution of this work is the application of PCA to ASTER multispectral data to enhance lithological boundaries and identify spectrally separable rock units in an underexplored part of the Dharwar Craton. This study uses ASTER VNIR--SWIR bands to derive principal components, select those that most clearly express lithological differences, and validate the interpreted patterns using published geological information and field observations. This approach helps refine lithological understanding of the Holenarasipur Schist Belt and evaluates the usefulness of PCA-based remote sensing in complex Precambrian geological settings.

2. Geology of the Study Area

The study area covers the Holenarasipur Schist Belt, one of the important supracrustal belts of the Western Dharwar Craton in southern India. It lies in Hassan district, Karnataka, and forms part of an Archean cratonic terrain containing rock assemblages dated between about 3.3 and 2.5 Ga [27][18]. The belt is known for its trident-shaped geometry and well-preserved supracrustal sequences. It includes exposures of the Sargur Group and the Bababudan Group of the Dharwar Supergroup, which occur to the south and north of the Hemavati River, respectively [7][28].

The study region extends approximately between 12º 30′ - 13º 15′ N latitude and 76º 00′ - 76º 25′ E longitude (see Figure 1). The Sargur Group is mainly composed of high-grade supracrustal rocks, whereas the Bababudan Group

consists of volcano-sedimentary sequences that have undergone variable degrees of metamorphism [7][18]. The belt contains medium- to high-grade metamorphic mineral assemblages, including kyanite, staurolite, garnet, and mica [32]. Major lithologies (see Figure 2) include schist, amphibolite, quartzite, metamorphosed basalt, and ultramafic units. Some ultramafic bodies preserve spinifex-textured komatiitic affinities and are locally altered to serpentinised peridotite [4][18].

Ultramafic rocks in the belt are locally associated with layered chromite mineralisation, suggesting magmatic differentiation processes [28]. Pegmatite bodies are also common in and around the Holenarasipur Schist Belt. They are important because they contain mica-bearing minerals and occur with quartz, feldspar, biotite, garnet, zircon, and apatite [24][40]. The close association of supracrustal rocks, ultramafic bodies, granitoids, pegmatites, and metamorphic assemblages produces strong lithological complexity in the area. This complexity makes the belt suitable for evaluating whether ASTER-derived PCA components can improve lithological discrimination and support geological mapping.

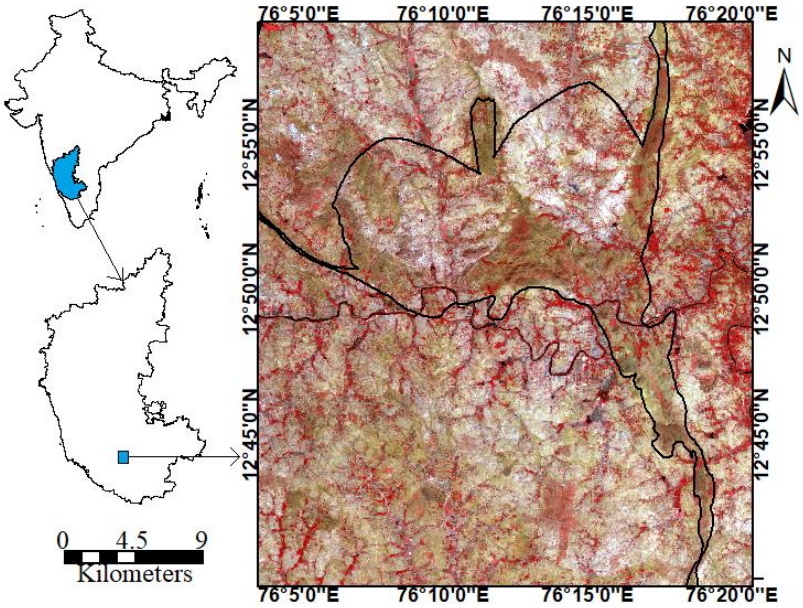

Fig. 1 Holenarsipura Schist Belt boundary overlaid on ASTER image (RGB: 3, 2, 1)

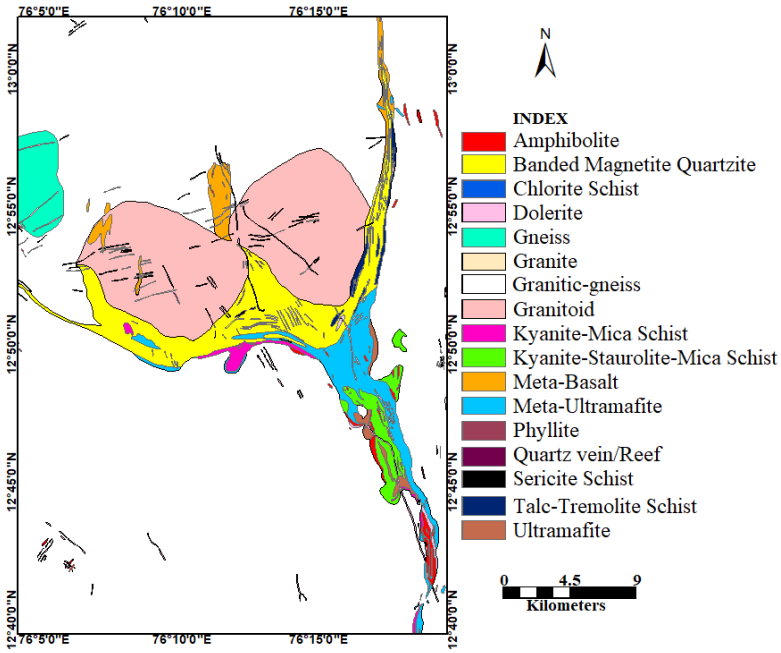

Fig. 2 Showing the geology of the study area

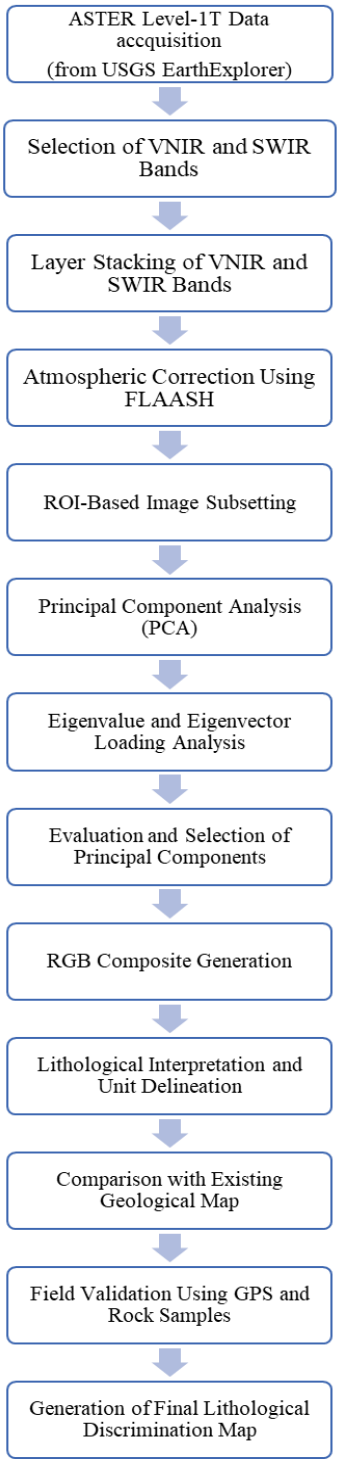

Fig. 3 Showing the methodological workflow adopted in this study

3. Materials and Methods

3.1. Aster Dataset and Preprocessing

The Advanced Spaceborne Thermal Emission and Reflection Radiometer (ASTER) is a 14-band multispectral sensor that records data from the visible to thermal infrared region of the electromagnetic spectrum, approximately between 0.53 and 11.65 µm [2][1]. The sensor includes three Visible and Near-Infrared (VNIR) bands, Six Shortwave Infrared (SWIR) bands, and five thermal infrared (TIR) bands. The VNIR and SWIR bands are particularly useful for lithological studies because they respond to variations in iron-bearing, hydroxyl-bearing, carbonate, silicate, and magnesium-rich minerals [29][31].

For the present study, an ASTER Level-1T terrain-corrected scene covering the Holenarasipur Schist Belt was obtained from the United States Geological Survey (USGS) Earth Explorer platform. The dataset was acquired on 15 February 2004. Level-1T products are radiometrically calibrated and geometrically corrected using ground control points and digital elevation information, making them suitable for spatial analysis and geological interpretation [2][41]. The image was subset to the study area and checked against Survey of India toposheets and available geological maps. Standard pre-processing steps included layer stacking of the VNIR and SWIR bands, geometric verification, radiometric correction, and visual inspection for cloud cover and scene quality. The VNIR and SWIR bands were used for PCA because these bands contain the most relevant spectral information for discriminating the lithological assemblages exposed in the study area. Image processing was carried out in ENVI Classic, while final cartographic preparation and map layout were completed in ArcMap [14][13].

The methodological workflow adopted in the present study (see Figure 3) and the major processing and validation steps are described in the following subsections.

3.2. Principal Component Analysis

Principal Component Analysis (PCA) was applied to the ASTER VNIR and SWIR bands to reduce spectral redundancy and enhance lithological differences. Multispectral bands commonly contain overlapping information, especially in adjacent wavelength regions, which can make geological interpretation difficult [36][19]. PCA addresses this issue by transforming correlated spectral bands into a new set of uncorrelated variables known as Principal Components (PCs) [6]. These components are derived from the eigenvalues and eigenvectors of the covariance matrix of the selected ASTER bands [20][36].

In this study, nine ASTER bands were included in the PCA: three VNIR bands and six SWIR bands. The transformation produced nine principal components. The first components generally contain the highest proportion of total variance, whereas later components may contain either subtle spectral information or noise. Therefore, all generated components were examined individually rather than selecting components only on the basis of variance percentage. This step was important because lithologically meaningful

information may occur in lower-order components when the spectral response of a mineral group is distinct but spatially limited [10][39].

3.3. Evaluation of Principal Components and RGB Composite Generation

Each principal component was assessed by considering its eigenvalue, percentage variance, image contrast, and band loading pattern. In PCA, an eigenvalue represents the amount of spectral variance contained in a principal component, while percentage variance shows how much of the total dataset variability is explained by that component [20][36]. These measures help identify components that contain strong overall image information, but they should not be used alone because high variance may also represent broad brightness, topographic, vegetation, or albedo effects rather than lithological contrast [10][39]. An eigenvector defines the direction of a principal component in the transformed spectral space and shows how the original ASTER bands are mathematically combined to produce each PC image [20][36].

Band loading values are the coefficients of the original ASTER bands within an eigenvector; they indicate the relative contribution of each band to a particular component. Therefore, careful evaluation of the loading values helps identify the dominant spectral response associated with each principal component and relate it to possible lithological units. Bands with high positive or high negative loading values can be interpreted as strongly influential, whereas values close to zero indicate weak contribution. Differences in band response reflect variations in mineralogy and surface properties, which can improve discrimination of lithological formations in the study area [10][39]. For this reason, eigenvalue distributions were interpreted together with component loadings, image contrast, and field evidence to evaluate lithological variability in the multispectral ASTER data [16][36][23]. Previous ASTER-based studies have also shown that PCA loading interpretation is useful for identifying hydrothermal alteration zones, lithological contacts, and mineral assemblages because VNIR and SWIR bands are sensitive to diagnostic absorption features of specific minerals [31][3]. Recent ASTER-based lithological studies further show that PCA interpretation becomes more reliable when eigenvalues, percentage variance, loading patterns, image contrast, field observations, and geological maps are evaluated together [5][12][30][21]

After the individual PC images and loading values were evaluated, the components showing the clearest geological contrast were selected for RGB composite generation. The RGB composite was interpreted by examining colour contrast, spatial continuity, and correspondence with mapped geological trends. Isolated colour patches without geological continuity were treated cautiously because they may represent local surface effects, mixed pixels, or vegetation cover rather than separate rock units.

3.4. Field Validation and Geological Comparison

Field validation was carried out to assess the reliability of the PCA-based lithological interpretation. Existing 1:50,000 scale geological maps prepared by the Geological Survey of India and downloaded from the Bhukosh Geological Survey of India portal were used as the main geological reference. Survey of India toposheets No. 57D/01 and 57D/02 were used as base maps to locate representative lithological units, plan field traverses, and relate field sites to the mapped topographic and geological framework.

Representative rock units were selected by comparing the PCA-derived images with the available geological maps and field accessibility. During fieldwork, sample locations were recorded using a handheld Global Positioning System (GPS), and the observed lithologies were compared with the PCA-derived lithological patterns and RGB composites. This comparison helped evaluate whether the spectral responses observed in the PCA outputs corresponded to known lithological boundaries and field-verified rock types.

The validation was based on the agreement among field observations, GSI geological maps, Survey of India toposheets, and spectral patterns visible in the PCA products. This integrated approach helped distinguish geologically meaningful PCA responses from possible image artefacts, mixed pixels, local surface effects, vegetation influence, or isolated tonal variations.

3.5. Mapping of Lithological Units Using Principal Component Analysis

Lithological mapping was carried out by combining PCA image interpretation, band loading analysis, RGB composite interpretation, existing geological information, and field validation. The purpose of this step was not to classify every pixel automatically, but to identify the principal components and colour composite patterns that best expressed the main lithological contrasts in the Holenarasipur Schist Belt. This approach was adopted because the area contains narrow, discontinuous, and partly mixed rock units, where a single image band may not separate the lithologies clearly.

4. Results and Discussion

4.1. Interpretation of PCA Loadings for Lithological Discrimination

The PCA transformation produced nine principal components from the ASTER VNIR–SWIR bands (see Figure 4). The eigenvalues and loading values are shown in Table 1. The eigenvalue of PC-1 was the highest, showing that it contained the largest part of the total image variance. However, PC-1 was not treated as the best component for individual lithological mapping because high variance can

also represent general scene brightness, topography, vegetation, and background albedo effects. Therefore, the component selection was not based only on eigenvalues.

The loading values were used to understand the spectral contribution of each ASTER band to each. principal component. A high positive or high negative loading indicates that the corresponding band has a strong influence on that component. Opposite signs between bands are important because they show spectral contrast between different wavelength regions. This contrast can be related to differences in rock composition, especially where VNIR bands respond to iron-bearing minerals and SWIR bands respond to hydroxyl and magnesium-bearing minerals.

Table 1. Principal Component Analysis of ASTER Image

Band/ PC	PCA-1	PCA-2	PCA-3	PCA-4	PCA-5	PCA-6	PCA-7	PCA-8	PCA-9
Band-1	-0.225629	-0.310319	-0.364143	-0.445912	-0.355571	-0.352224	-0.319180	-0.290662	-0.290694
Band-2	0.044572	0.156136	-0.901847	-0.025356	0.154087	0.152099	0.164982	0.199580	0.213861
Band-3	-0.608806	-0.670159	-0.020023	0.267157	0.192695	0.181208	0.140484	0.095953	0.097760
Band-4	0.567993	-0.570676	0.092703	-0.463352	0.098765	0.062413	0.108739	0.185055	0.262115
Band-5	0.498541	-0.309606	-0.210616	0.612079	0.017329	0.061716	-0.177101	-0.297322	-0.335747
Band-6	-0.072570	0.089408	0.024677	-0.297452	0.444320	0.604193	-0.398804	-0.418383	-0.033092
Band-7	0.000440	-0.020653	-0.002182	0.205594	-0.453182	0.102794	-0.412856	-0.148676	0.740813
Band-8	0.000843	-0.015459	0.009334	-0.058966	-0.566913	0.630920	-0.017869	0.392763	-0.349520
Band-9	-0.005701	-0.004940	0.004194	0.074748	0.280098	-0.196440	-0.691496	0.626434	-0.081913
Eigen values	0.156076	0.002797	0.001538	0.000175	0.000138	0.000037	0.000030	0.000026	0.000016

PC-1 had the highest eigenvalue and therefore contained the largest proportion of the total image variance. It showed strong positive loadings in Band 4 (0.567993) and Band 5 (0.498541), and a strong negative loading in Band 3 (-0.608806). This opposite response between the VNIR and SWIR bands indicates a broad spectral contrast across the scene. But, PC-1 was not interpreted as the main lithological component because the first component can also include general brightness, topographic effects, vegetation influence, and background albedo variation [36][19]. In this study, PC-1 was therefore used mainly as supporting information for recognising broad lithological heterogeneity and separating the schist belt from the surrounding background.

PC-2 showed strong negative loadings in Band 3 (-0.670159) and Band 4 (-0.570676), with additional negative contributions from Band 1 (-0.310319) and Band 5 (-0.309606). This loading pattern indicates a strong VNIR-SWIR contrast and is useful for enhancing iron-bearing and ferruginous lithologies. In the study area, banded magnetite quartzite showed the clearest response in PC-2. This interpretation is consistent with the iron-rich character of this unit and with the sensitivity of VNIR bands to iron-bearing minerals, while SWIR bands help separate ferruginous rocks from silicate-dominated units [17][29][31].

PC-3 was dominated by a strong negative loading in Band 2 (-0.901847), with positive contributions from Band-3 (0.304593) and Band 4 (0.259472). This indicates a visible and SWIR spectral contrast. In the PCA images, PC-3 helped distinguish relatively bright felsic lithologies, especially Peninsular gneiss and granitoid, from darker schistose units. The field samples of gneiss and granitoid are rich in quartz and feldspar, which explains their brighter response, whereas schistose rocks mostly contain mica-rich minerals like biotite, muscovite, and chlorite that produce darker tonal responses. Banded magnetite quartzite showed an intermediate response because of the combined presence of magnetite and quartz. Thus, PC-3 was useful for recognising major felsic and schistose lithological contrasts in the study area [9].

PC-4 had a high positive loading in Band 5 (0.612079), moderate positive loading in Band 3 (0.267157), and negative loading in Band 4 (-0.463352), with additional contribution from Band 6 (-0.297452). This band relationship

is important because the SWIR region is sensitive to hydroxyl- and magnesium-bearing minerals. Talc, schist, and meta-ultramafite were therefore linked mainly to PC-4. These units are expected to show Mg-OH and OH-related spectral behaviour because of minerals such as talc, serpentine, amphibole, mica, and other hydrous silicates. PC-4 was therefore useful for mapping ultramafic and hydroxyl-bearing lithologies, although the interpretation was checked against field observations to avoid over-interpreting isolated tonal patches [9] [29] [31].

PC-5 showed positive loading in Band 6 (0.444320) and negative loadings in Band 7 (-0.453182) and Band 8 (-0.566913). These bands occur in the SWIR region and may contain information related to Mg-OH absorption. In the present study, PC-5 supported the interpretation of talc schist and meta-ultramafite, but its spatial contrast was weaker than PC-4. Therefore, PC-5 was treated only as a secondary component and was not used as the main basis for lithological separation.

PC-6 had strong positive loadings in Band 6 (0.604193) and Band 8 (0.630920), but its eigenvalue was low, and the image did not show a consistent relationship with mapped lithological units or field observations. PC-7, PC-8, and PC-9 also had very low eigenvalues and mostly showed weak and inconsistent tonal patterns. These higher-order components were therefore considered to contain limited geological information for this study and were not used for the final lithological composite [15][20][36].

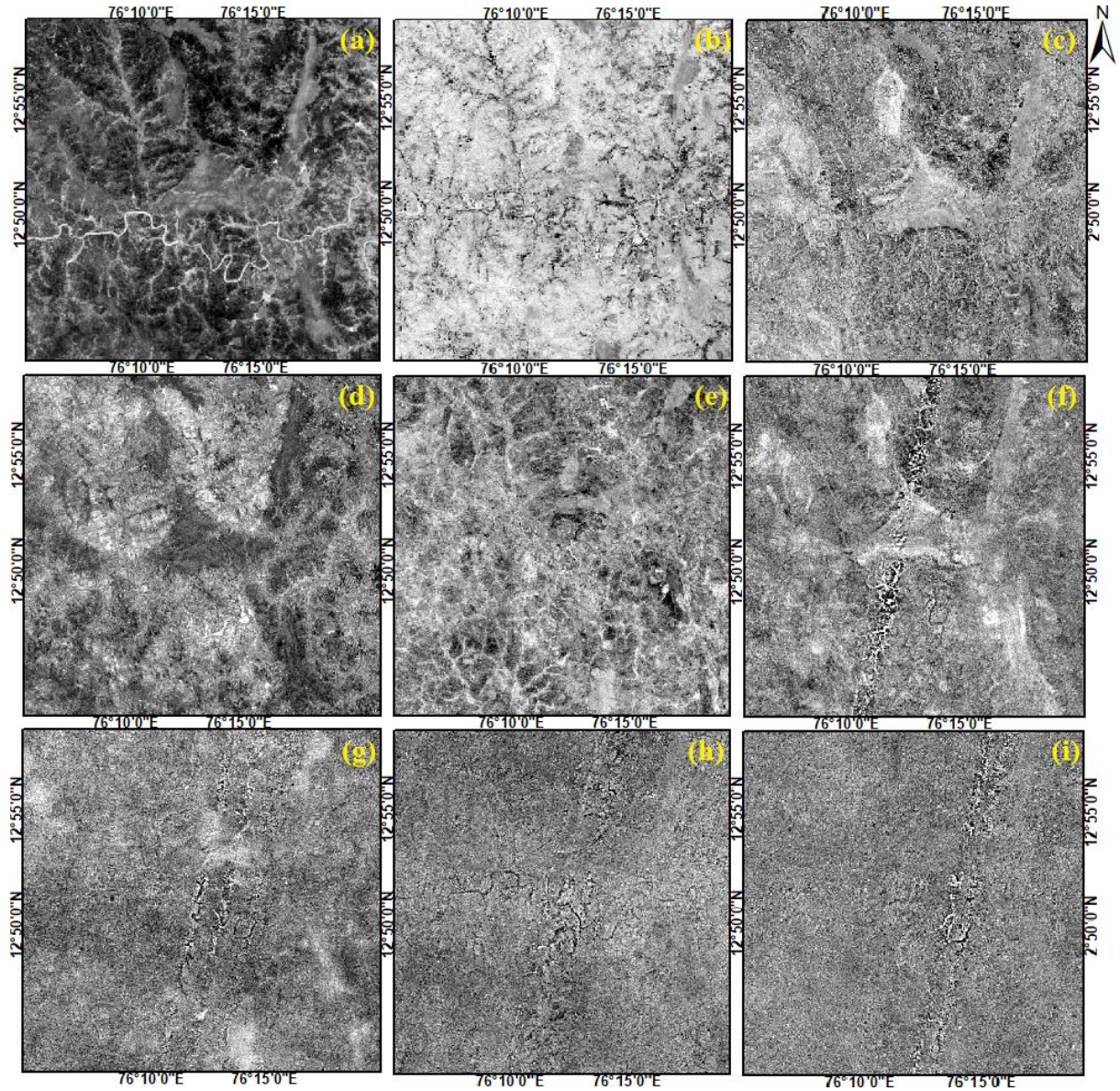

Fig. 4 The PCA image of Principal Components 1 to 9 of the Holenarasipur Schist belt, (a) PC-1; (b) PC-2; (c) PC-3; (d) PC-4; (e) PC-5; (f) PC-6; (g) PC-7; (h) PC-8; (i) PC-9

4.2. Lithological Interpretation and Field Comparison

The final lithological interpretation was based on the selected PCA components, the RGB composite, existing geological information, and field observations. PC-2, PC-3, and PC-4 were used as the main components because they showed the clearest relation with iron-bearing, felsic, and hydroxyl- or magnesium-bearing lithologies, respectively. The RGB composite of PC-2, PC-3, and PC-4 (see Figure 5) was validated by the field visits. Table 2 summarises the representative field samples collected (See Figure 6), their coordinates, the most useful PC response, and the PCA interpretation.

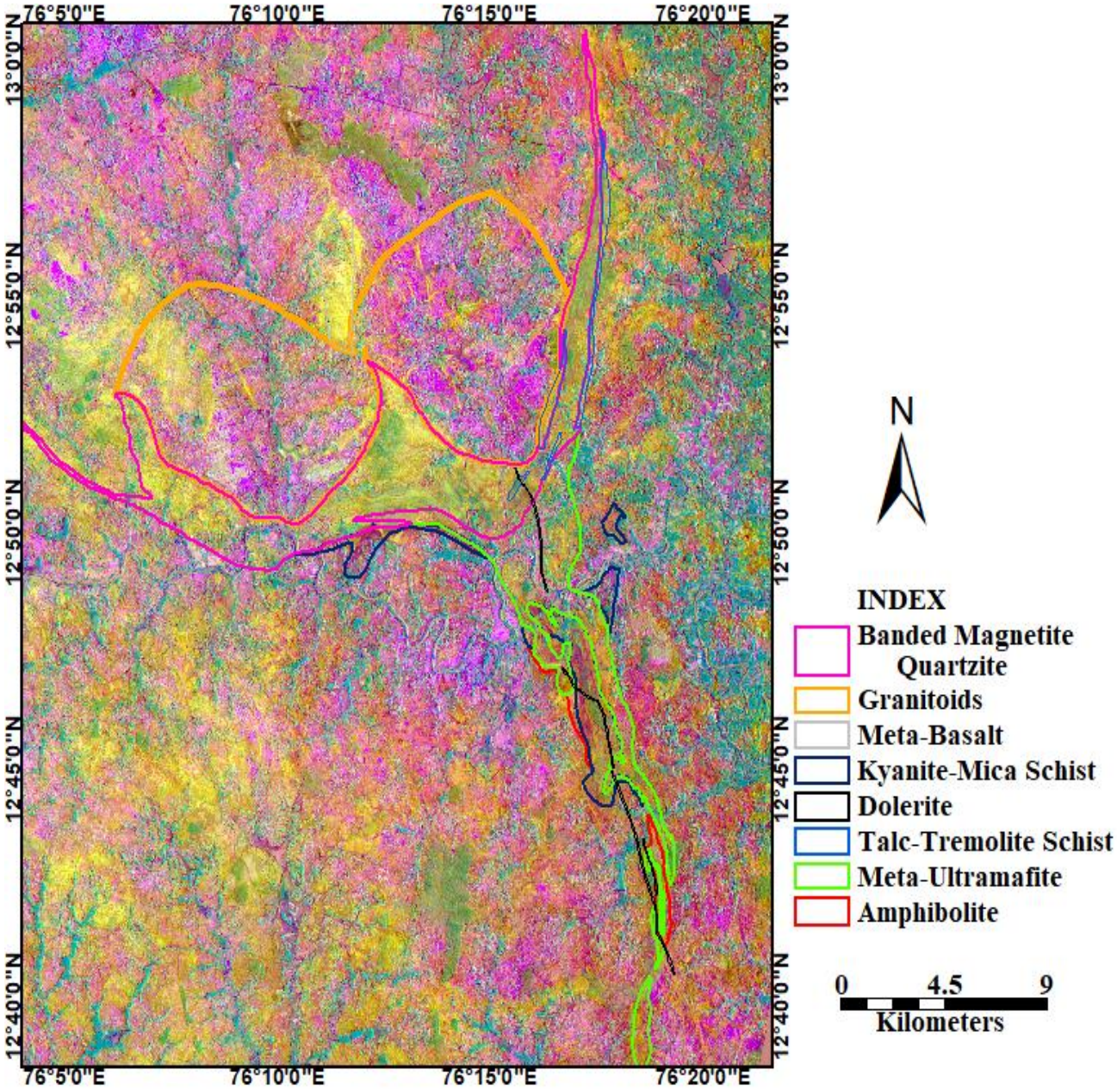

Fig. 5 The RGB combination of Principal Components (R: PC2, G: PC3, B: PC4), to help discriminate the lithologies of the study area

Hand specimen observations were used to support the lithological interpretation and to relate the field samples to the ASTER-PCA response. Banded magnetite quartzite was linked to PC-2 because of its iron-bearing character. Peninsular gneiss and granitoid were related mainly to PC-3 because their quartz–feldspar rich composition produced relatively bright felsic responses. Kyanite-mica schist showed a relation with PC-3 and PC-4 because it is schistose and contains hydroxyl-bearing mica minerals. Talc schist and meta-ultramafite were associated with PC-4, with secondary support from PC-5, because of their Mg–OH-bearing mineral assemblages.

Amphibolite and dolerite dyke were retained in the interpretation Table 2 because they were observed in the field and are compositionally relevant to the ASTER VNIR–SWIR bands. Amphibolite contains amphibole and plagioclase, with Fe–Mg and hydroxyl-bearing mineral phases. Dolerite dyke is a mafic intrusive unit with Fe–Mg silicate minerals. However, both units were not interpreted as independently separable PCA classes. Their weak, overlapping PCA response is likely due to narrow exposure, mixed pixels, and spectral similarity with adjacent mafic, schistose, and ultramafic rocks. This interpretation avoids over-estimating the ability of PCA to map lithologies that are not clearly visible as separate tonal units.

The RGB composite (see Figure 5) was prepared using PC-2, PC-3, and PC-4, which improved the visual separation of the main lithological units. PC-2 contributed information on iron-bearing rocks, PC-3 helped distinguish brighter felsic gneissic and granitoid units, and PC-4 enhanced Mg–OH- and OH-bearing lithologies.

The composite was therefore useful for recognizing the broad lithological pattern of the Holenarasipur Schist Belt, especially where the PCA response agreed with mapped lithological boundaries and field sample locations.

Table 2. Field-observed lithologies and their relationship with selected ASTER-PCA components.

Sample No.	Sample Collected	Location (Latitude and Longitude)	Best Identified PC	PCA interpretation
1.	Peninsular gneiss	12 °52’ 19.17” N, 76°14’ 08.96” E	PC-3; supported by PC-1	Brighter felsic unit separated from schistose rocks.
2.	Granitoid	12° 53’ 38.86” N, 76° 15’ 54.28” E	PC-3; supported by PC-1	Brighter quartz–feldspar-rich unit
3.	Banded magnetite quartzite	12° 53’ 14.96” N, 76°16’ 21.82” E	PC-2	Clearly enhanced iron-bearing unit.
4.	Kyanite-mica schist	12° 49’ 59.63” N, 76°13’ 56.45” E	PC-3 and PC-4	Contrasts with felsic units; partly overlapping response.
5.	Amphibolite	12° 40’ 10.30” N, 76°18’ 31.32” E	Weak PC-2 and PC-4	Field-identified, not independently separated in PCA.
6.	Dolerite dyke	12° 44’ 16.89” N, 76°18’ 08.78” E	Weak PC-2 and PC-4	Field-identified mafic dyke; overlapping PCA response.
7.	Talc schist	12° 54’21.59” N, 76°16’23.75” E	PC-4; secondary PC-5	Highlighted as Mg–OH-bearing unit.
8.	Meta-ultramafite	12° 47 ’45.10” N, 76°16’ 21.82” E	PC-4; secondary PC-5	Best expressed by OH/Mg-sensitive SWIR contrast.

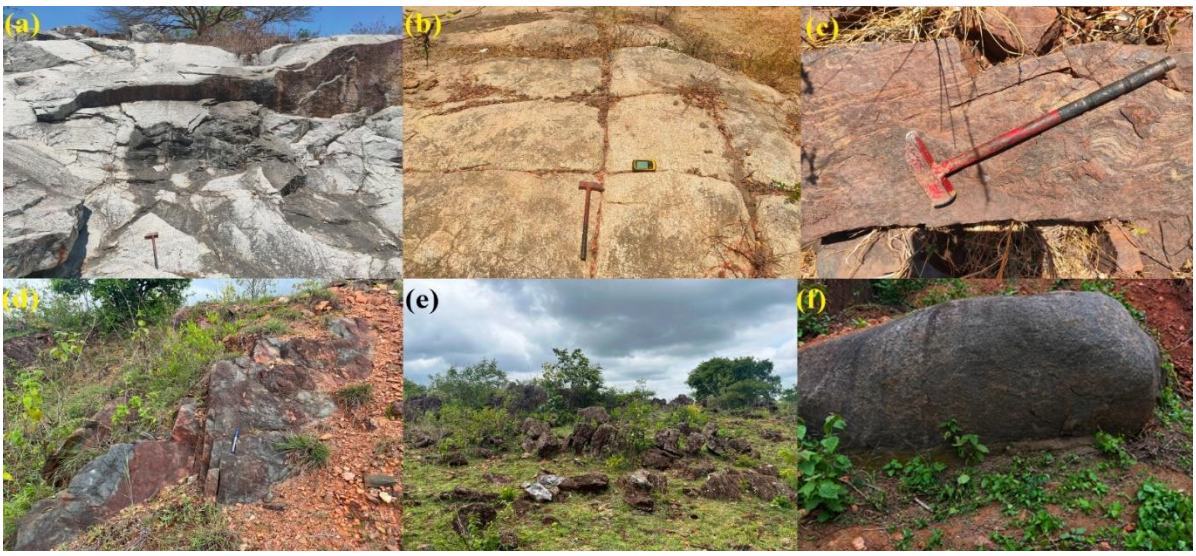

Fig. 6 Field photographs showing (a) Peninsular Gneiss; (b) Granitoid with orthogonal joint system; (c) Banded Magnetite Quartzite; (d) Kyanite-Chlorite Schist; (e) Amphibolites; (f) Dolerite

4.3. Discussion

The results show that PCA improved the visual separation of the main rock units in the Holenarasipur Schist Belt. The most useful information came from PC-2, PC-3, and PC-4, rather than from PC-1 alone. This is important because PC-1 mainly represents the largest overall variance in the image, which may include brightness, surface cover, and topographic effects. In contrast, the lower-order components showed clearer links with specific lithological groups. This supports earlier work showing that PCA can reduce repeated spectral information and bring out useful geological contrasts in multispectral data [15][36][16]. Recent studies also show that ASTER-based enhancement methods remain useful for lithological and mineralogical mapping when they are combined with geological interpretation and field evidence [5][12][21][30].

PC-2 was most useful for recognising banded magnetite quartzite and other iron-bearing units. This interpretation is supported by the strong response of the banded magnetite quartzite in the PCA image and by the known sensitivity of VNIR wavelengths to iron-bearing minerals [17][29] The result is also consistent with ASTER-based studies from India, where PCA and related enhancement methods have helped distinguish lithological units and mineralised zones using VNIR--SWIR spectral differences [34][25][35].

PC-3 mainly enhanced the felsic units, especially the Peninsular gneiss and granitoid. These rocks are rich in quartz and feldspar, which helps explain their brighter response compared with darker schistose rocks. PC-4 was more useful for talc schist and meta-ultramafite because these rocks contain hydroxyl- and magnesium-bearing minerals such as talc, serpentine, amphibole, mica, and other hydrous silicates. This agrees with previous studies showing that ASTER SWIR bands are useful for detecting hydroxyl-, silicate-, carbonate-, and mafic--ultramafic lithologies [9] [29][43][31].

The geological setting of the Holenarasipur Schist Belt explains why different principal components highlighted different lithologies. The area contains supracrustal rocks, ultramafic bodies, granitoids, gneisses, pegmatites, and metamorphic assemblages within a limited space. Ultramafic rocks are locally associated with chromite mineralisation, while pegmatite bodies contain mica-bearing minerals and occur with quartz, feldspar, biotite, garnet, zircon, and apatite [28][24][40]. Because these rock groups have different mineral compositions, they respond differently in the VNIR--SWIR bands. Therefore, the PCA output reflects real geological and mineralogical variation, not only image contrast.

The PC-2--PC-3--PC-4 RGB composite was useful because it combined the strongest responses from iron-bearing, felsic, and hydroxyl- or magnesium-bearing rocks in one image. This made the broad lithological pattern easier to interpret and helped compare the satellite-based results with field observations. Similar results have been reported from other geological settings, where ASTER-PCA, band ratios, and related enhancement methods improved the mapping of carbonate, silicate, mafic--ultramafic, iron-rich, and altered rocks [3][43][31][5][12][30][21]. These recent studies are important because they show that ASTER data are still useful for lithological mapping, even when newer classification methods and higher-resolution datasets are available. The agreement between this study and earlier work shows that ASTER-PCA is a practical method for lithological mapping in complex Precambrian terrains when the image interpretation is checked with field data.

4.4. Limitations of ASTER-PCA Analysis

Although ASTER-PCA improved lithological discrimination in the study area, the method has some limitations. The spatial resolution of ASTER VNIR and SWIR bands can produce mixed pixels where rock units are narrow, discontinuous, or closely interlayered. This is one reason why amphibolite and dolerite dyke were identified in the field but were not clearly separated as independent PCA classes. Their spectral response may also overlap with nearby mafic, schistose, and ultramafic rocks.

Surface conditions can also affect the PCA results. Weathering, soil cover, vegetation, slope, and moisture may change the spectral response of exposed rocks and reduce the contrast between lithological units. In metamorphic terrains such as the Holenarasipur Schist Belt, different rocks may also show similar spectral behaviour because of metamorphic overprinting or shared mineral phases. These factors can make some lithological boundaries less clear in the PCA images [36][19][23].

For these reasons, the PCA images should be viewed as interpretation aids rather than final geological maps. In this study, their reliability was assessed by comparing the image patterns with selected field samples, existing geological information, and the known mineralogical character of the mapped units. This approach provides field-based support for the interpretation, but it does not represent a full numerical accuracy assessment. A separate study with more ground-control points would be needed to estimate the mapping accuracy of each lithological unit in detail. Further separation of subtle mineralogical variations may also require higher spatial resolution data, hyperspectral imagery, or supervised classification methods, particularly where lithologies are narrow or spectrally similar [26][38][21]

The RGB composite generated using PC-2, PC-3, and PC-4 provided a clear visual separation of the major lithological units and improved the interpretation of spatial geological patterns in the study area. Field observations and representative rock samples supported the satellite-based

interpretation, showing that the PCA results are geologically meaningful when checked with ground information. Overall, the study demonstrates that ASTER-PCA is a practical, reliable, and cost-effective approach for lithological mapping in complex Precambrian terrains. However, the method should be used together with field validation and geological knowledge, especially where rock units are narrow, mixed, weathered, or spectrally similar.

5. Conclusion

This study shows that PCA applied to ASTER VNIR--SWIR data is useful for lithological discrimination in the Holenarasipur Schist Belt. The PCA transformation reduced repeated spectral information and enhanced important geological contrasts that were not clearly visible in the original multispectral bands. Among the derived components, PC-2, PC-3, and PC-4 were the most useful for mapping the main lithological variations. PC-2 highlighted iron-bearing formations such as banded magnetite quartzite, PC-3 enhanced quartz--feldspar-rich felsic rocks such as gneiss and granitoid, and PC-4 helped identify hydroxyl- and magnesium-bearing units such as talc schist and meta-ultramafite.

Conflict of Interest

The authors declare that there is no conflict of interest regarding the publication of this paper.

References

[1] Henry Draper, *The Draper Catalogue of Stellar Spectra: Photographed with the 8-Inch Bache Telescope as a Part of the Henry Draper Memorial*, University Press, vol. 27, pp. 1-388, 1890. [Google Scholar]

[2] Alexander Friedman, "On the Curvature of Space," *Journal of Physics*, vol. 10, no. 1, pp. 377-386, 1922. [CrossRef] [Google Scholar] [Publisher Link]

[3] Albert Einstein, *The General Theory of Relativity*, The Meaning of Relativity, Springer, Dordrecht, pp. 54-75, 1936. [CrossRef] [Google Scholar] [Publisher Link]

[4] Pierre-Simon Laplace, *Exposition of the World System*, 2nd ed., Cambridge University Press, vol. 2, 2010. [Google Scholar] [Publisher Link]

[5] Georges Lemaître, "A Homogeneous Universe of Constant Mass and Increasing Radius Accounts for the Radial Velocity of Extragalactic Nebulae," *Annals of the Scientific Society of Brussels*, vol. A47, pp. 49-59, 1927. [Google Scholar]

[6] Edwin Hubble, and Richard C. Tolman, "Two Methods of Investigating the Nature of the Nebular Red-shift," *Astrophysical Journal*, vol. 82, pp. 302-337, 1935. [Google Scholar]

[7] Edwin Hubble, "The Luminosity Function of Nebulae. I. the Luminosity Function of Resolved Nebulae as Indicated by their Brightest Stars," *Astrophysical Journal*, vol. 84, pp. 158-179, 1936. [Google Scholar]

[8] Robert Geroch, "What is a Singularity in General Relativity?," *Annals of Physics*, vol. 48, no. 3, pp. 526-540, 1968. [CrossRef] [Google Scholar] [Publisher Link]

[9] Robert Geroch, "*Singularities*," *Relativity: Proceedings of the Relativity Conference in the Midwest*, held at Cincinnati, Ohio, pp. 259-291, 1970. [CrossRef] [Publisher Link]

[10] Robert Geroch, Liang Can-bin, and Robert M. Wald, "Singular Boundaries of Space-times," *Journal of Mathematical Physics*, vol. 23, no. 3, pp. 432-435, 1982. [CrossRef] [Google Scholar] [Publisher Link]

[11] George Gamow, and Edward Teller, "On the Origin of Great Nebulae," *Physical Review Journals Archive*, vol. 55, no. 7, pp. 654-657, 1939. [CrossRef] [Google Scholar] [Publisher Link]

[12] Hermann Bondi, and Ian W. Roxburgh, *Cosmology*, Courier Corporation, 2010. [Google Scholar]

[13] Edward Arthur Milne, "Relativity, Gravitation and World Structure," *Nature*, vol. 135, no. 3417, pp. 635-636, 1936. [CrossRef] [Google Scholar] [Publisher Link]

[14] Edward Arthur Milne, "Kinematic Relativity," *Journal of the London Mathematical Society*, vol. s1-15, no. 1, pp. 44-80, 1940. [CrossRef] [Google Scholar] [Publisher Link]

[15] Hermann Bondi, and Thomas Gold, "The Steady-State Theory of the Expanding Universe," *Monthly Notes: of the Royal Astronomical Society*, vol. 108, no. 3, pp. 252-270, 1948. [CrossRef] [Google Scholar] [Publisher Link]

[16] Arthur Stanley Eddington, "The Expanding Universe," *Nature*, vol. 132, no. 3332, pp. 406-407, 1933. [CrossRef] [Google Scholar] [Publisher Link]

[17] Paul Adrien Maurice Dirac, "A New basis for Cosmology," *Proceedings of the Royal Society of London. Series A. Mathematical and Physical Sciences*, vol. 165, no. 921, pp. 199-208, 1938. [CrossRef] [Google Scholar] [Publisher Link]

[18] Pascual Jordan, "The Origin of the Stars," *Stuttgart*, 1947. [Google Scholar]

[19] Fred Hoile, "A New Model for the Expanding Universe," *Monthly Notices of the Royal Astronomical Society*, vol. 108, no. 5, pp. 372-382, 1948. [CrossRef] [Google Scholar] [Publisher Link]

[20] Roger Penrose, ""Golden Oldie": Gravitational Collapse: The Role of General Relativity," *General Relativity and Gravitation*, vol. 34, no. 7, pp. 1141-1165, 1969. [CrossRef] [Google Scholar] [Publisher Link]

[21] Robert M. Wald, *Space, Time, and Gravity: The Theory of the Big Bang and Black Holes*, 2nd ed., University of Chicago Press, 1992. [Google Scholar] [Publisher Link]

[22] Hendrick B.G. Casimir, "On the Attraction Between Two Perfectly Conducting Plates," *Proceedings of the Koninklijke Nederlandse Akademie van Wetenschappen / C*, vol .51, 1948. [Google Scholar]

[23] Tamara M. Davis, and Charles H. Lineweaver, "Expanding Confusion: Common Misunderstanding of Cosmological Horizons and the Superluminal Expansion of the Universe," *Publications of the Astronomical Society of Australia*, vol. 21, no. 1, pp. 97-109, 2004. [CrossRef] [Google Scholar] [Publisher Link]

[24] Stephen Willian Hawking, "The Occurrence of Singularities in Cosmology," *Proceedings of the Royal Society of London. Series A. Mathematical and Physical Sciences*, vol. 294, no. 1439, pp. 511-521, 1967. [CrossRef] [Google Scholar] [Publisher Link]

[25] Stephen Willian Hawking, "Particle Creation by Black Holes," *Communications in Mathematical Physics*, vol. 43, no. 3, pp. 199-220, 1975. [CrossRef] [Google Scholar] [Publisher Link]

[26] Stephen Willian Hawking, "The Unpredictability of Quantum Gravity," *Communications in Mathematical Physics*, vol. 87, no. 3, pp. 395-415, 1982. [CrossRef] [Google Scholar] [Publisher Link]

[27] Erik Curiel, "The Analysis of Singular Spacetimes," *Philosophy of Science*, vol. 66, no. S3, pp. S119-S145, 1999. [CrossRef] [Google Scholar] [Publisher Link]

[28] George F.R. Ellis, and Bernd G. Schmidt, "Singular Space-Times," *General Relativity and Gravitation*, vol. 8, no. 9, pp. 915-953, 1977. [CrossRef] [Google Scholar] [Publisher Link]

[29] Nikodem Poplawski, "Universe in a Black Hole with Spin and Torsion," *The Sixteenth Marcel Grossmann Meeting*, pp. 1327-1336, 2023. [CrossRef] [Google Scholar] [Publisher Link]

[30] Nikodem Poplawski, "Universe in a Rotating Black Hole and Preferred Axis," *arXiv e-prints*, 2019. [CrossRef] [Google Scholar] [Publisher Link]

[31] Marek S. Żbik, "The Universe as Two-Dimensional Membrane on the Event Horizon of Singularity," *SSRG International Journal of Geoinformatics and Geological Science (SSRG-IJGGS)*, vol. 7, no. 2, pp. 21-27, 2020. [CrossRef] [Google Scholar] [Publisher Link]

[32] Marek S. Żbik, "Non-Expanding Universe Model," *SSRG International Journal of Geo-Informatics and Geological Science*, vol 10, no. 1, pp. 25-28, 2023. [CrossRef] [Google Scholar] [Publisher Link]

[33] Kip Thorn, Richard H. Price, and Douglas A. MacDonald, Black Holes: The Membrane Paradigm, New Haven: Yale University Press, 1986. [Online]. Available: https://ui.adsabs.harvard.edu/abs/1986bhmp.book.....T/abstract

[34] Fritz Zwicky, "Republication of: the Redshift of Extragalactic Nebulae," *General Relativity and Gravitation*, vol. 41, no. 1, pp. 207-224, 2008. [CrossRef] [Google Scholar] [Publisher Link]

[35] Vera C. Rubin, W. Kent Ford Jr, and Norbert Thonnard, "Extended Rotation Curves of Highluminosity Spiral Galaxies. IV - Systematic Dynamical Properties, SA through SC," *Astrophysical Journal*, vol. 225, no. 1, pp. L107-L111, 1978. [Google Scholar]

[36] Chelsea Papineau, *Sudbury SNOLAB makes Scientific Breakthrough in Monitoring Nuclear Power,* CTV News, 2023. [Online]. Available: https://www.ctvnews.ca/northern-ontario/article/sudbury-snolab-makes-scientific-breakthrough-in-monitoring-nuclear-power/

[37] Douglas Clowe et al., "A Direct Empirical Proof of the Existence of Dark Matter," *The Astrophysical Journal*, vol. 648, no. 2, pp. L109-L113, 2006. [CrossRef] [Google Scholar] [Publisher Link]

[38] Vazquez-Gonzalez, and T. Matos., "Dark Matter in the Universe: Challenges and Perspectives," *Mexican Physics Magazine E*, vol. 54, no. 2, pp.193-202, 2008. [Google Scholar] [Publisher Link]

[39] Evalyn Gates, *Einstein's Telescope: The Hunt for Dark Matter and Dark Energy in the Universe*, Einstein's Telescope, WW Norton and Company, 2010. [Google Scholar] [Publisher Link]

[40] J. Richard Gott III et al., "A Map of Universe," *The Astrophysical Journal*, vol. 624, no. 2, pp. 463-484, 2005. [CrossRef] [Google Scholar] [Publisher Link]

[41] Diana Scognamiglio et al., "An Ultra-High-Resolution Map of (Dark) Matter," *Nature Astronomy*, vol. 10, no. 4, pp. 573-582, 2026. [CrossRef] [Google Scholar] [Publisher Link]

[42] Stephen Willian Hawking, *Black Holes and Thermodynamics*, Science Center, Harvard University, 1982. [Google Scholar]